Transcriptomic landscape reveals germline potential of porcine skin-derived multipotent dermal fibroblast progenitors

Wen-Xiang Liu
Qingdao Agricultural University
Chun-Xiao Li
Qingdao Agricultural University
Xin-Xiang Xie
Qingdao Agricultural University
Wei Ge
Qingdao Agricultural University
Tian Qiao
Qingdao Agricultural University
Xiao-Feng Sun
Anqiu Women and Children's Hospital
Wei Shen
Qingdao Agricultural University
shunfeng cheng (sfcheng@qau.edu.cn)
Qingdao Agricultural University https://orcid.org/0000-0002-2836-2762

Research Article

Keywords: Skin-derived stem cells, Single-cell transcriptomes, Multipotent dermal fibroblast progenitors, Primordial germ cell-like cells, MAPK signalling pathway

Posted Date: March 24th, 2023

DOI: https://doi.org/10.21203/rs.3.rs-2701295/v1

Version of Record: A version of this preprint was published at Cellular and Molecular Life Sciences on July 22nd, 2023. See the published version at https://doi.org/10.1007/s00018-023-04869-7.

Abstract

According to estimations, approximately about 15% of couples worldwide suffer from infertility, in which individuals with azoospermia or oocyte abnormalities cannot be treated with assisted reproductive technology. The skin-derived stem cells (SDSC) differentiation into primordial germ cell-like cells (PGCLC) is one of the major breakthroughs in the field of stem cell intervention for infertility treatment in recent years. However, the cellular origin of SDSC and its dynamic changes in transcription profile during differentiation into PGCLC *in vitro* remain largely undissected. Here, the results of single-cell RNA sequencing indicated that porcine SDSC is mainly derived from multipotent dermal fibroblast progenitors (MDFP), which are regulated by growth factors (EGF/bFGF). Importantly, porcine SDSC exhibit pluripotency for differentiating into three germ layers and can effectively differentiate into PGCLC through complex transcriptional regulation involving histone modification. Moreover, this study also highlights that porcine SDSC-derived PGCLC specification exhibit conservation with the human primordial germ cells lineage and that its proliferation is mediated by the MAPK signalling pathway. Our findings provide substantial novel insights into the field of regenerative medicine in which stem cells differentiate into germ cells *in vitro*, as well as potential therapeutic effects in individuals with azoospermia and/or defective oocytes.

Introduction

The World Health Organization's official statistics indicate that there are 48 million couples and 186 million individuals worldwide who are currently affected by infertility, with this number expected to continue increasing [1]. Although existing assisted reproductive technology has solved the fertility needs of some infertile patients, there is no effective treatment for individuals with azoospermia or oocyte abnormalities [2]. In recent decades, scientists have been exploring the possibility of using stem cells to produce primordial germ cells (PGC) or functional gametes (eggs and sperm) in the laboratory, known as *in vitro* gametogenesis [3, 4]. This research is motivated by the potential to use these PGC or gametes to generate offspring, as well as the possibility of using them to study early human development and to model diseases. Several types of stem cells that have been explored for this purpose, including embryonic stem cells (ESC) [5], induced pluripotent stem cells (iPSC) [6], and adult stem cells (ASC) [7]. However, the ability to produce functional gametes from stem cells *in vitro* is still a subject of ongoing research and has not yet been successfully achieved in pigs or humans.

Although breakthroughs in mice have shown that ESC and iPSC can differentiate into germ cells which successfully produced offspring *in vitro* [5, 8], significant differences in gene expression patterns between mice and human PGC are increasingly reported [9–11]. In contrast, the similarities between porcine genetics, anatomy, and physiology and those of humans render the pig an ideal model for the investigation of human medical conditions [12, 13]. Recent studies have shown that the specification of the pig germline exhibits conservation with that of the human lineage, meaning that the process is closely aligned in both species [10, 14]. These findings highlight the importance of studying the pig as an animal model for germline programming to determine the therapeutic feasibility for individuals with subfertility.

Considering the limited availability of ESC and the potential carcinogenicity of iPSC [15, 16], scientists have directed their attention to skin-derived stem cells (SDSC), a subtype of ASC, which offer a plethora of clinical applications while circumventing the ethical concerns commonly associated with other types of stem cells [7, 17, 18]. Such cells are isolated from the skin of mice, pigs and humans and induced to differentiate into primordial germ cell-like cells (PGCLC) *in vitro* [7, 17, 18], which are key to further differentiation of gamete-like cells to mimic *in vivo* gametogenesis. However, one unanswered question is which type, or types, of cells in the skin do the SDSC originate from. Previous studies indicated that SDSC can differentiate into a variety of cells in specific induction mediums, including astrocytes, adipocytes, liver cells, and germ cells [19]. There is a hypothesis among some researchers that the ability for multipotent differentiation observed in the skin is attributed to the presence of diverse stem cell populations within the epidermis, dermis, and hair follicles [20]. Other researchers have suggested that SDSC may be derived from cells during early embryonic development [21], present in the dermis, and capable of generating cells of different lineages [22]. The emergence of single-cell RNA sequencing (scRNA-seq) has greatly advanced the understanding of cellular heterogeneity and cell fate transition through the ability to precisely dissect these processes at the individual cell level [23, 24]. Moreover, the cell heterogeneity analysis of mouse and goat skin development provides a reference for understanding the cell origin of porcine SDSC [23, 24]. In summary, the cellular origin of SDSC derived from porcine fetal skin remains unknown and promises to be thoroughly examined and deciphered using scRNA-seq.

Another concern is that the inefficiency in forming PGCLC constrains its applicability as a treatment option for infertility caused by the loss of germ cells. As early as 2009, Linher and colleagues used porcine SDSC to induce differentiation into PGCLC, and the induction efficiency was only about 1.4% [25]. Subsequently, other studies reported that some endogenous metabolites, including luteinizing hormone (LH), melatonin (MLT), and retinoic acid (RA), can significantly augment the proliferation of porcine PGCLC [7, 26, 27]. Until now, detailed analysis of the mechanisms involved during SDSC-induced PGCLC formation and proliferation have not been reported. There is an urgent need for this analysis prior to the therapeutic application of *in vitro* gametogenesis.

In this study, we used scRNA-seq to identify the cellular origin of the SDSC from porcine skin and further analysed their multipotent differentiation potential and germline potential to form PGCLC *in vitro*. Moreover, this work also investigated porcine SDSC-derived PGCLC lineage specific expression and the mechanisms by which endogenous metabolites promote the proliferation of PGCLC. Overall, these findings underscore the germline potential of dermal fibroblast progenitor derived SDSC and that they have the potential to be an effective means of preserving fertility.

Materials And Methods

Animals, human, and administration

The porcine fetuses were procured from Wanfu Group Co. Ltd (Qingdao, Shandong, China). The CD-1 mice utilized were procured from Vital River Laboratory Animal Technology Co. Ltd (Beijing, China).

Additionally, the CAG/eGFP transgenic mice strain was graciously provided by Dr. Xiao Yang of the Institute of Biotechnology in Beijing. Human fetal genital ridge tissue samples were obtained from Anqiu Women and Children's Hospital (Shandong, China). In accordance with national guidelines, written informed consent was obtained from all study participants, and the study was reviewed and approved by the Ethics Committee of Anqiu Women and Children's Hospital as well as the Ethical Committee of Qingdao Agricultural University (QAU; Agreement No. 2020-018).

Epidermal growth factor (EGF, R&D Systems, 2028-EG, USA) and basic fibroblast growth factor (bFGF, PeproTech, 100-18B, USA) were dissolved in DMEM/F12 (Gibco, C11330, USA) containing 1% BSA and working solutions of EGF (20 ng/ml) and bFGF (40 ng/ml) were prepared in DMEM/F12 medium [25]. Melatonin (MLT, Sigma, M5250, Germany) was dissolved in anhydrous ethanol to 200 mM, and then diluted to 25 μM in differentiation medium as working solution [7]. Luteinizing hormone (LH, Sigma, L5269) was dissolved in DMEM medium to achieve a working concentration of 400 mIU for differentiation induction [26]. Retinoic acid (RA, Sigma, R4643) was dissolved with DMSO to 10mM storage solution, and then diluted to 5 μM in differentiation medium as working solution [27]. U0126 (Abcam, ab120241, UK) was dissolved in DMSO to 50 mM concentrated storage, and then diluted to 10 μM in differentiation medium for experimental use [27].

Dissociation of porcine skin and generation of SDSC spheres

The porcine SDSC culture method used in this experiment has been described above [7, 26, 27]. Dorsal skin was collected from female pig fetuses on gestation days 35–45 (E35-E45). Use a scalpel to cut into tissue blocks and wash with PBS (Solarbio, T8200, Beijing, China). Then, the tissue blocks were cultured with SDSC medium [DMEM/F12 (1:1), 20 ng/ml EGF, 40 ng/ml bFGF, 1% penicillin-streptomycin (Solarbio, P1400) and 1% B27 (Gibco, 17504044)] in 10 cm culture dishes (Sarstedt, Montreal, Canada). After 4 days, the tissue blocks were collected into a 15 ml centrifuge tube and the cells were mechanically dissociated using a 1 ml pipette. The single-cell suspension was continued in SDSC medium, and the medium was replaced every four days. The resulting SDSC spheres were harvested after 12 days of culture for further procedures. The diameters of SDSC colonies (four groups: control, EGF, bFGF, EGF and bFGF) were measured using ImageJ (V1.48) software (NIH, MD, USA).

Induction of porcine PGCLC

Porcine SDSC *in vitro* induction of porcine PGCLC was performed as previously [7, 26, 27]. In brief, SDSC clones are separated into single cells and inoculated into 60 mm cell dishes (Corning, 430166, USA) according to the density of 1×10^5 cells. The differentiation medium [DMEM (Gibco, C11995500BT), 5% FBS, 5% porcine follicular fluid, 1% GlutaMAX™ Supplement (Thermo Fisher Scientific, 35050061, USA), 0.1 mM 2-mercaptoethanol (2-ME, Sigma, M-7522), 1% non-essential amino acids solution (NEAA, Thermo Fisher Scientific, 11140-050), 1% sodium pyruvate] was changed every four days. The PGCLC was collected for follow-up experiments after about 16 days of differentiation.

Strategies for mouse SDSC differentiation of PGCLC in vitro

Previously published protocols detailed the isolation of mouse skin and the generation of SDSC clones [17]. The dorsal skin of newborn mice expressing the CAG/eGFP transgene was collected and subsequently dissected into smaller pieces using scissors. The single cell suspension was obtained using trypsin-EDTA solution (Sorlabio, T1300, China) in an incubator for 25 min and a 40 μm cell strainer (Biologix, 15-1040, USA). The individual cells obtained were cultured, with the medium being replaced every four days. After 12 days of cultivation, the generated SDSC spheres were harvested for subsequent experimentation.

The protocol and culture regimen for inducing PGCLC from mouse SDSC were executed in strict compliance with previously established protocol [17]. EpiLC was induced by P2 mouse SDSC, which was dissociated from single cell suspension and seeded into 24-well plates at 5×10^5 cells/well in EpiLC induction medium [17]. EpiLC colonies were dissociated into single cells after four days and were pipetting at a concentration of 5×10^5 cells/ml and plated on mitogenic inactivated MEF feeding cells for PGCLC induction in PGCLC differentiation medium [17, 28]. The half medium was replaced every two days and the generated suspended PGCLC were harvested for subsequent experimentation after about 12 days.

Single cell cDNA library preparation and sequencing

Dorsal skin tissue from at least three fetal pigs was separated into small pieces and subsequently digested in incubator with a trypsin-EDTA solution for 25 min to obtain single cell suspensions. The P2 SDSC spheres were dissociated by the above method to obtain single cell suspension. Samples were then filtered using a 40 μm cell filter and washed using with DMEM basic containing 0.1% BSA. We constructed a single cell cDNA library using Chromium single cell 3' Reagent Kit (10×Genomics, PN-1000075, USA). Cells with more than 90% viability were captured using the 10× Genomics Chromium controller (10× Genomics, DNBSEQ-T7, USA).

scRNA-seq data preprocessing and data visualization

The standard agreement to use CellRanger (v3.0.2) software for UMI does a comparison and quantitative. Seurat (v3) R package was used to conduct downstream quality control and visualization analysis of the processed expression matrix [29]. During quality control, low-quality cells are filtered using the default parameters in Seurat and the data is consolidated using the FindIntegrationAnchors function in the Seurat package. Then, the RunUMAP and FindClusters functions were used for reduction and cluster recognition. Single-cell trajectory inference was performed using the slingshot R package to infer dynamic gene expression along a pseudotime axis [30]. Everything else defaults to the official guidelines.

Hematoxylin-eosin (H&E) staining

The skin was fixed overnight at 4°C with 4% PFA solution (Sorlabio, P1110). The following day, the fixed tissue was dehydrated in an ethanol solution and treated with xylene for 30 min. Then, the sample was

embedded in paraffin. The slices were cut into 5 μm slices using Leica RM2255 microtome (Leica, RM2235, Germany), and the samples were transferred to adhesive slide. After the slides were dewaxed and rehydrated, they were stained with hematoxylin solution for 7 min and then rinsed with distilled water twice for 5 min. After rinsing with 1% HCl-ethanol solution for 3–5 sec, immediately rinse with 45°C water for 5 min. After dehydration, dye with 1% eosin ethanol solution and rinse with anhydrous ethanol for 10 min. Finally, the sheet was sealed with a neutral resin and photographed under microscope (Olympus, BX51, Japan).

Immunofluorescence (IF) staining, immunohistochemistry (IHC) staining, and immunocytochemistry (ICC) staining

The IF staining method used in this experiment has been described in recent studies [31]. In short, the slides were rehydrated and antigenic repair was performed. In brief, the slide was incubated with boiled 0.01 M sodium citrate buffer (pH = 6.0) for 10 min. After cooling to room temperature, the slide was closed with a blocking buffer (0.5 M Tris-HCl buffer containing 3% BSA and 10% goat serum (BOSTER, AR0009, China). Subsequently, then primary antibody and the secondary antibody were added and incubated. Details of the antibodies used in this experiment are shown in Table S6. The nucleus was then stained by DAPI. The image was taken under a confocal microscope (Leica Microsystems GmbH, TCS SP5 II). For IHC, in order to block endogenous peroxidase activity, 3% hydrogen peroxide was treated for 10 min, followed by color development with DAB kit (ZSGB-BIO, ZLI-9017, China).

ICC is used to detect protein localization and expression levels in cells. In short, cells are fixed with 4% PFA solution (Sorlabio, P1110), and then the cells are coated on a slide to dry. Then, PBST (PBS with 0.5% Triton X-100) was permeated for 10 min, and PBST containing 10% goat serum was sealed at room temperature for 30 min. After closure, the primary antibody was added. Then, the slides were rinsed with PBS containing 1% BSA (Solarbio, A8020) for three times, and an appropriate secondary antibody was added according to the species source of the primary antibody at 37℃ for 45 min. Details of primary and secondary antibodies are listed in Table S6. The nucleus was stained with DAPI or PI. Finally, confocal microscopy was used for image acquisition.

CCK-8 cell proliferation assay

The CCK-8 cell viability assay kit (Solarbio, CA1210) was used in this experiment. According to the standard requirements of the testing kit, the 10% CCK-8 solution was incubated in an incubator at 37℃ for 2 h. Subsequently, the absorption value at 450 nm wavelength was detected with a microplate reader (Bio-Rad, iMarkTM, USA).

Cell cycle analysis

Flow cytometry was used to measure DNA amount and cell cycle distribution. Briefly, the SDSC spheres for 4 groups (control, EGF, bFGF, EGF and bFGF) were digested into single cells by trypsin-EDTA solution, and fixed overnight at 4℃ in 70% ethanol. After the cells were washed with pre-cooled PBS, stained with the prepared propidium iodide staining solution (containing RNase A, Beyotime, C1052, China), and

incubated at 37℃ for 30 min away from light. Finally, FACS Calibur flow cytometer (Becton Dickinson, FACS Calibur, USA) was utilized to measure 20 000 cells per sample, and then used FlowJo v10 software for analysis.

Flow cytometry analysis

For single staining, the collected genital ridges and PGCLC (mouse) were digested into single cells and fixed with pre-cooled 80% methanol. They were then incubated with primary antibody (Table S6) for 60 min and secondary antibody (Table S6) for 45 min at 37℃. The samples were detected by flow cytometry and analyzed by WinMDI 2.9 software. For co-staining, the samples were incubated with primary antibodies including SOX17, PCNA (Table S6) and then incubated with secondary antibodies including fluorescein isothiocyanate (FITC) and Cyanine3 (CY3) conjugated antibodies (Table S6) for 45 min at 37°C. The cells suspension was detected by flow cytometer and the data was analyzed by FlowJo V10 software.

Teratoma formation and analysis

To investigate whether SDSC has properties similar to pluripotent stem cells, SDSC colonies were collected and transplanted to kidney capsules in SCID/Beige immune-deficient mice (Vital River Laboratory Animal Technology Co., Ltd, Beijing) for 10 weeks of ectopic development. The solid tumor was then observed, removed, fixed, sliced, and stained by H&E for histological analysis.

PCR and real time quantitative PCR (RT-qPCR)

Total RNA was extracted from tissues (solid tumor) and cells (SDSC, PGCLC) using RNAiso Plus (TaKaRa, 9109, Japan) and cDNA reverse transcription kit (SparkJade, AG0304, China) was used to synthesize the cDNA according to directions. PCR using Taq DNA Polymerase (TransGen, AP101, China) was performed in a 50 μl reaction volume according to instructions. Details of all primers are listed in Table S7. The amplified products were separated by electrophoresis using 2% agarose gel.

RT-qPCR used SYBR Premix Ex Taq™ II (Vazyme, Q711-02, China). The reaction was performed by Roche 480 Light Cycler RT-qPCR instrument (Roche, Germany) as previously described [32]. The RT-qPCR reactions were done in 20 μl reaction volume containing: 2 μl cDNA, 10 μl SYBR Premix Ex Taq™ II (2×), 7.2 μl RNase-free water, and 0.4 μl (10 μM) forward and reverse primers respectively. All primers are listed in Table S7. Real-time PCR and $2^{-(\triangle\triangle Ct)}$ methods were used to measure relative gene expression [33]. Each sample was amplified by PCR three times, and porcine GAPDH as housekeeping gene.

Western blotting (WB) analysis

Firstly, the cells were collected by centrifugation in a 1.5 ml centrifuge tube, and the RIPA lysate (Beyotime, P0013C, China) was added for ice cracking. Protein was boiled with 5× SDS-PAGE Sample Loading Bufer (Beyotime, P0015L, China) for 5 min to denaturate protein. Then 12% SDS-PAGE was used for electrophoresis, 80 V for 30 min, then 120 V for 90 min. Bio-Rad Trans-Blot (Bio-Rad, Hercules, California, USA) was used to transfer proteins to polyvinadiene fluoride membranes (PVDF; Millipore,

ISEQ00010, USA) for 150 min at 200 mA constant flow. Blocking was performed with TBST buffer (containing 5% skim milk powder) at room temperature for 2 h, the protein bands were incubated with primary antibody at 4℃ overnight and secondary antibody at room temperature for 75 min. All antibodies are listed in Table S6. Chemiluminescence was performed with BeyoECL Plus kit (Beyotime, P0018, China) and used AlphaView SA software for gray analysis of protein bands.

RNA sequencing (RNA-seq) analysis

Novogene Company (Beijing, China) was responsible for RNA extraction, library construction and sequencing of RNA-seq in this experiment. Three duplicate samples were detected in each group to ensure the reliability of the results. The data were quality-controlled, recounted and base-corrected with fastp in Linux, then compared with the reads in a pig reference genome using STAR, and finally tallied the number of reads using featureCounts. Differentially expressed genes (DEGs) with DESeq2 analysis, and $|log2FoldChange| > 1$ and P-value < 0.05 as the threshold for significant differences in gene expression.

Gene ontology (GO) and Kyoto Encyclopedia of Genes and Genomes (KEGG) enrichment

GO and KEGG enrichment of DEGs and representative gene sets were performed using ClusterProfiler software [34]. GO items and KEGG pathways with a P-value of less than 0.01 were regarded as significantly enriched.

Statistical analysis

The experimental data were expressed in the form of mean ± standard deviation, and each group of experiments was repeated at least 3 times. One-way analysis of variance was used to analyze data followed by Tukey's test for multiple comparisons using GraphPad Prism 8 software. *: $0.01 < P < 0.05$ indicates a statistically significant difference and **: $P < 0.01$ indicates a highly significant difference.

Results

Dissection of cellular heterogeneity of porcine skin and P2 SDSC at single-cell resolution

According to published protocols [7, 26, 27], the SDSC were mechanically separated from the porcine skin and cultured to passage two (P2) (Figure S1A). To analyze the cellular heterogeneity, a single cell suspension of porcine skin and the P2 SDSC were prepared, barcoded following single cell capture, and subjected to scRNA-seq (Fig. 1A). Subsequently, low-quality or doublet cells were removed, resulting in the remained number of cells being 11 417 in the skin and 9 730 in SDSC sample, and the mean number of genes expressed in each sample were 1 763 and 2 684, respectively (Figure S1B and S1C). After that, we integrated two samples to characterize cell identity and 16 cell clusters were produced by uniform manifold approximation and projection (UMAP) for dimension reduction (Fig. 1B, S1D, S1E, and Table S1). Notably, there are significant differences in cell heterogeneity between the skin and SDSC samples.

The SDSC were mainly composed of clusters 0, 1, 5, 6 and 9 (Fig. 1C), suggesting that SDSC come from one or several types of cells in the skin.

Further, as shown in Fig. 1D and S1F, we defined the seven major categories in UMAP using a series of canonical marker genes. These were dermal fibroblasts (clusters 0 to 9) with *LUM*, *COL1A1*, *POSTN* and *APOE* expression [23, 35–37], endothelial cells (clusters 11) with *KDR* and *PRCAM1* expression [38], melanocytes (clusters 15) with *PLP1* and *DCT* expression [39], muscle cells (clusters 10) with *PAX7* and *ITGA7* expression [40], pericyte cells (clusters 12) with *KCNJ8* and *FRMD3* expression [41, 42], macrophage (clusters 13) with *MMP9* and *CD68* expression [43], and dendritic cells (clusters 14) with *CCR7* and *LAMP3* expression [44]. Hierarchical clustering indicated that 5 clusters (0, 1, 5, 6, and 9) of cells mainly derived from SDSC were clustered together with dermal fibroblasts of skin origin (Fig. 1E). After batch correlation, the cells with origin from the SDSC sample were all expressing dermal fibroblast markers, and the other 11 clusters were mainly comprised of cell populations derived from the skin (Fig. 1F). In addition, the H&E staining categorized the tissue in the dermal condensate phase [45], when dermal fibroblast populations of skin origin expressed *PDGFRA* and *LRIG1*, which are specific markers of dermal fibroblast progenitors [22] (Fig. 1G). Collectively, these data demonstrated that SDSC mainly derived from dermal fibroblast progenitors.

Growth factors (EGF/bFGF) promote the formation of large SDSC colonies in vitro

To capture the differentiation trajectories of dermal fibroblast, Slingshot analysis along the UMAP shows the root and terminal branches of the cell fates of dermal fibroblasts (Fig. 2A). Further, the cell groups of origin of SDSC were divided into three groups, including clusters 0/5, cluster1 and clusters 6/9 (Fig. 2B). However, the analysis of shared genes showed that the cell clusters of SDSC origin were divided into two distinct groups, with clusters 0/1/5 and clusters 6/9 sharing more genes, respectively (Figure S2A and S2B). The GO analysis showed that clusters 6/9 high-expression gene enrichment in “RNA localization, regulation of cell cycle checkpoint, and positive regulation of cell cycle phase transition”; and clusters 0/1/5 high-expression gene enrichment in “response to growth factor and regulation of fibroblast proliferation” (Fig. 2C). Considering that more than 80% of the total number of SDSC were at clusters 0/1/5 (Fig. 1F), we then evaluated the effect of growth factors on the proliferation of the SDSC *in vitro*.

We first confirmed that dermal fibroblasts express growth factor receptors (*EGFR* and *FGFR1/2/3*) and dermal fibroblast progenitor markers (*PDGFRA* and *LRIG1*) by porcine skin scRNA-seq (Fig. 2D, S2C-S2E). In addition, immunohistochemistry (IHC) showed that EGFR and FGFR1 were expressed in the porcine skin cells (Fig. 2E and 2F). Next, removing EGF or/and bFGF from the culture medium, we found that the ability of SDSC to generate large colonies and cell viability were significantly reduced (Fig. 2G-2I). This may be related to the growth factors (EGF/bFGF) stimulating the cell cycle of SDSC and promoting the entry of the S phase and G2/M phase transition (Fig. 2J). Taken together, these results further confirmed that growth factors (EGF/bFGF) are essential for the proliferation and formation of large SDSC colonies *in vitro*.

Ectopic development of SDSC derived from dermal fibroblast progenitors was multipotent in vivo

To investigate whether SDSC have properties similar to pluripotent stem cells, we transplanted these SDSC colonies under the kidney capsules of immune-deficient mice, and solid tumors formed after 10 weeks of transcplantation (Fig. 3A). Subsequently, PCR analysis revealed that three germ layers markers, including the ectodermal marker genes *NOTCH1* and *GFAP* [46, 47], mesodermal marker genes *KDR* and *HAND1* [48, 49] and endodermal marker genes *AFP* and *FOXA2* [46, 50], were identified in ectopic developed SDSC derived solid tumors (Fig. 3B-3D). Importantly, we confirmed by H&E staining that tumors contained tissues derived from three germ layers, including ectoderm-derived neuroepithelium, mesoderm-derived muscle and adipose, and endoderm-derived original kidney (Fig. 3E). Collectively, these results indicated that SDSC derived from multipotent dermal fibroblast progenitors (MDFP) have the pluripotency to differentiate into three germ layers.

Dissection of transcriptional profiles with PGCLC induction from SDSC by RNA sequencing (RNA-seq)

We next investigated the germline potential of MDFP derived SDSC and designed a scheme showing four samples (skin, P0_0: SDSC on day 0 of P0, P2-4: SDSC on day 4 of P2, and PGCLC) collection for transcriptional analysis (Fig. 4A). According to published protocols [7, 26, 27], cells that exhibit a suspended and shiny appearance following 16 days of differentiation induction are considered PGCLC (Fig. 4B). The principal component analysis (PCA) plot and correlation heatmap plot of RNA-seq data demonstrated transcriptomes for the four groups changed as they developed from the skin to PGCLC (Fig. 4C and 4D). To investigate the drivers of germline progression, we analyzed differentially expressed genes (DEGs) in the three processes, including skin to P0_0, P0_0 to P2_4, and P2_4 to PGCLC (Fig. 4E-4G and Table S2). Among them, 2 018, 1 451, and 2 445 DEGs play a decisive role in the process of skin to P0_0, P0_0 to P2_4, and P2_4 to PGCLC, respectively (Fig. 4H).

We then used Gene Set Enrichment Analysis (GSEA) to analyze the main GO biological processes of DEGs for the three processes, and found that “Skin development” and “Epithelial cell differentiation” were inhibited while “Mitochondrial translation” and “Ribosome assembly” were activated during the skin to P0_0 process; “Regulation of cell differentiation”, “Apoptotic process”, “Regulation of protein modification process”, and “Negative regulation of cell population proliferation” were inhibited during the P0_0 to P2_4 process; “Regulation of cell differentiation”, “MAPK cascade”, “Response to cytokine”, and “Regulation of protein modification process” were activated during the P2_4 to PGCLC process (Fig. 4I). These results suggest that germline induction processes of SDSC require complex transcriptional regulation.

To analyze the dynamic changes of genes as they developed from skin to PGCLC, the heatmap showed the representative genes of each group, which were 2 061 genes in the skin group, 366 genes in the P0_0 group, 624 genes in the P2_4 group, and 1 571 genes in the PGCLC group (Fig. 5A and Table S3). Enrichment analysis demonstrated that P0_0 high expression genes were related to “regulation of cellular response to growth factor stimulus” and “regulation of fibroblast growth factor receptor signaling pathway” (Fig. 5A), which was consistent with the results of growth factor deprivation inhibiting the proliferation of SDSC (Fig. 2). Moreover, PGCLC high expression genes were mostly enriched in the

biological processes of “positive regulation of cell migration”, “positive regulation of MAPK cascade”, “reproductive system development”, and “gamete generation” (Fig. 5A), which strongly indicated that SDSC had the potential of germline differentiation.

Further, compared with the skin group, the expression levels of pluripotency related markers (*MYC*, *SOX9*, *KLF2*, *KLF4*, *STAT3*, and *TCF7L1*) [9, 51–54] were significantly up-regulated in the P0_0 SDSC group (Fig. 5B). SOX9, MYC, and SSEA1 were expressed in cells after culturing to P2_4 by SDSC (Fig. 5C). Similarly, compared with the P2_4 group, the expression levels of the PGC specialized related genes (*SOX17*, *TFCP2L1*, *PRAME*, *CD38*, *PRDM1*, *ALPL*, *RNF17*, and *TFAP2C*) [7, 9, 14, 51] were all significantly increased in the PGCLC group (Fig. 5D). Among them, *SOX17*, *TFCP2L1*, *PRAME*, and *CD38* were activated in the PGCLC, while not detected in the P2_4 SDSC (Fig. 5E), indicating that these genes are essential for germline induction. Immunofluorescence (IF) staining showed that SOX17 and PRDM1 were mainly expressed in the suspended cells (Fig. 5F) that were considered as PGCLC. Moreover, western blotting results showed that H3K27me3 and H3K9me2 undergo progressive increase and erasure, respectively, during the PGCLC differentiation from MDFP derived P2_4 SDSC (Fig. 5G and 5H), which was consistent with the changes occurring in PGC specification of pigs *in vivo* [10, 14]. To summarize, MDFP derived SDSC have the germline potential to form PGCLC *in vitro*.

Porcine PGC shares gene expression pattern with human PGC but different from mice

According to a previously published protocol [17], mouse SDSC differentiation into PGCLC involves two main steps, induction of epiblast-like cells (EpiLC) followed by PGCLC specification (Fig. 6A). Similar to porcine SDSC derived PGCLC, mouse SDSC-induced PGCLC are suspened in culture (Fig. 6B). Similarly, mouse SDSC also expresses the pluripotent-related proteins SOX9, MYC, and CD34 (Fig. 6C). Although mouse PGCLC expressed PRDM1 as well as the porcine PGCLC, IF staining and flow cytometry analysis showed no SOX17 expression in the mouse SDSC-derived PGCLC (Fig. 6D and 6E). Considering the different expression patterns of PGC specialization in humans and mice [55, 56], this suggests that species-specific expression patterns are maintained during *in vitro* induction of PGCLC.

As shown in Fig. 7A, the timelines of the PGC origins and programming in human, pig, and mouse have been dissected [10, 14, 57]. To investigate the conservation of germline development in detail, genital ridges from E49 human embryo, E30 pig embryo and E12 mouse embryo were collected for subsequent experiments. Notably, SOX17-positive cells were detected in human and pig genital ridges using flow cytometry, but not in mouse genital ridges (Fig. 7B). Subsequently, we detected PGC gene expression patterns in the genital ridges by fluorescence staining. Importantly, we found that TFAP2C and PRDM1 positive cells were found in the genital ridges of all three species, and were co-located with the human PGC marker CD38 [9], porcine PGC marker OCT4 [14], and mouse PGC marker SSEA1 [58], respectively (Fig. 7C-7E). The difference was that SOX17 expression and SOX2 deletion were detected in the PGC of both pig and human, while the reverse was observed in the mouse PGC (Fig. 7C-7E). In addition, CD38 was not expressed in mouse PGC (Fig. 7E). Although no studies have shown whether porcine PGC

expresses the surface marker CD38, the scRNA-seq analysis of E45 and E55 porcine genital ridges showed that CD38 was expressed in about 10% of DDX4 or DAZL positive germ cells (Fig. 7F-7H and Table S4). Given the above, the germline specification between pigs and humans are conserved but different from that of mice, the implication is that pigs are an ideal animal model to simulate human PGC induction *in vitro* for the treatment of infertility.

PGCLC proliferation responds to endogenous metabolite stimulation through the MAPK signaling pathway

To obtain sufficient PGCLC for induction into germ cell-like cells, our previous studies have shown that endogenous metabolites can significantly promote PGCLC proliferation [7, 26, 27]. As shown in Fig. 8A, 400 mIU LH, 25 μM MLT or 5 μM RA were added during the PGCLC induction to explore the mechanisms of PGCLC proliferation. After 16 days of differentiation, more PGCLC were suspended in the treatment (LH/MLT/RA) group compared to the control group (Fig. 8B). The percentage of PGCLC that were double positive for SOX17 and PCNA, following treatment with LH, MLT, or RA, was more than threefold greater than that of the control group (Fig. 8C). Additionally, RNA-seq was employed to examine the distinct transcriptional characteristics of the control group, LH group, and MLT group. The PCA and correlation heatmap of the RNA-seq data revealed distinct transcriptomic profiles among the three groups (Fig. 8D and S3A). Subsequently, differential analysis showed that the LH and MLT groups had 4 456 and 1 339 up-regulated DEGs, and 3 736 and 2 140 down-regulated DEGs, respectively, compared with the control group (Figure S3B, S3C, and Table S5). This indicates that LH has a stronger effect on the PGCLC than the MLT. Enrichment analysis demonstrated that the GO biological process of DEGs corresponding to LH or MLT were all related to “regulation of cell proliferation” (Figure S3D and S3E), while their KEGG enrichment was significantly related to the “MAPK signaling pathway” (Fig. 8E). Interestingly, research has demonstrated that RA promotes PGCLC proliferation mediated by the MAPK signaling pathway [27]. The MAPK signaling pathway plays a crucial role in regulating proliferation by modulating key cell cycle regulators and other proteins that are related to cell proliferation [59]. Notably, LH stimulated more genes related to the MAPK signaling pathway than MLT (Fig. 8F), and corresponding cell cycle related genes were also activated in the LH and MLT groups (Fig. 8G). Supplementary findings confirmed that treatment with LH, MLT, or RA significantly elevated the levels of phosphorylation of MEK and ERK, as well as the expression of genes related to the cell cycle (Fig. 8H and 8I). Given that genes with high expression in PGCLC were found to be significantly enriched in the biological processes of “positive regulation of MAPK cascade” (Fig. 5A), suggesting that MAPK signaling pathway is the most central influencing factor in PGCLC proliferation in response to endogenous metabolite stimulation.

In order to determine the impact of the MAPK pathway on PGCLC proliferation, U0126, an inhibitor of the MAPK signaling pathway, was employed. After 16 days of differentiation, the 10 μM U0126 treatment group had fewer suspended PGCLC than the control group (Fig. 8J). The results obtained through flow cytometry demonstrated that U0126 was able to suppress the proliferation of PGCLC (Fig. 8K). These

findings suggest that the MAPK signaling pathway plays a direct role in the proliferation of PGCLC in response to treatment with endogenous metabolites (LH/MLT/RA).

Discussion

As early as 2001, researchers isolated a type of stem cell known as SDSC from skin tissue [60]. These cells possess the capability to be induced into cells derived from the three germ layers or germ cells *in vitro* when cultured under specific conditions [19]. Almost all researchers believe that skin-derived SDSC are heterogeneous and contain multiple stem cells localized in the epidermal, dermal, or hair follicle [20], and that these different stem cells may differentiate into different cell types. Additionally, the lack of well-conserved lineage markers in these stem cells hinders the ability to trace the origin of SDSCs and raises concerns about their pluripotency. This study uses scRNA-seq to demonstrate that porcine SDSC are mainly derived from MDFP (Fig. 1), which are the precursors of three types of papillary, reticular, and hypodermal fibroblast in the skin [21, 22].

The elegant studies in mice have identified distinct populations of cells during development and in the adult skin [22], suggesting that there may be significant differences in the SDSC isolated from skin samples at different ages. Published protocols indicate that fetal pig skin from gestational day 35–45 is used as source material for the SDSC isolation and *in vitro* germline potential [7, 25–27, 61]. At this stage, the dermis of porcine skin was mainly filled with MDFP [62], which is consistent with our conclusion. Notably, our attempt to separate SDSC from adult porcine skin found lower self-renewal capacity (data not shown), which may be related to a higher heterogeneity of the SDSC from adults [62]. In another study with mice, SDSC isolated from hair follicles alone showed high self-renewal and germline differentiation potential [63], suggesting that high or low cell heterogeneity affects the stability of the *in vitro* culture system. As a result, it is crucial to isolate the various stem cells present in adult skin to thoroughly evaluate their germline potential, and there is still much work to be done in this area.

In 2004, Dyce and colleagues isolated skin-originated stem cells (namely MDFP) from fetal pig and found that they had the potential to differentiate into cells resembling neurons, astrocytes, and adipocytes [61]. In fact, the MDFP possesses the capability to differentiate into the various fibroblasts, dermal papilla, arrector pili muscle cells, and adipocyte cells that make up the skin [21, 22]. Here, our strong results show that SDSC from MDFP is found to have the ability to differentiate into cells derived from three germ layers during the ectopic development under the kidney capsule (Fig. 3). Interestingly, we have shown for the first time that MDFP can differentiate into endoderm-derived original kidney, which may be related to the interior milieu in the kidney capsules.

Since the successful differentiation of PGCLC from SDSC *in vitro* in 2009 [7, 25–27], the transcriptional dynamics of this process have remained elusive. In the present study, transcription profiles with PGCLC induction from skin were analyzed for the first time by RNA-seq (Figs. 4 and 5). The P0_0 SDSC cells isolated from skin highly expressing pluripotent genes (*MYC*, *SOX9*, *KLF2*, *KLF4*, *STAT3*, and *TCF7L1*) [9, 51–54] and actively responded to growth factor (EGF/bFGF) stimulation to promote cell population

proliferation (Figs. 3 and 9). Subsequently, the differentiation program begins with the P2-4 SDSC, and begins to express PGC fate-related markers (*SOX17*, *TFCP2L1*, *PRAME*, *CD38*, *PRDM1*, *ALPL*, *RNF17*, and *TFAP2C*) [7, 9, 14, 51] accompanied by epigenetic changes in DNA methylation and histone modification [7, 27] (Fig. 9). Indeed, the specification of the pig rather than mouse germline exhibits conservation with the human lineage, for example, the expression of SOX2 and SOX17 [9, 10]. In this study, the results of the genital ridges staining of different species revealed that SOX17 was present exclusively in the porcine and human PGC, while the expression of SOX2 was the opposite (Fig. 7). Interestingly, SOX17 was not expressed in mouse SDSC derived PGCLC (Fig. 6), suggesting that species-specific expression was also present during *in vitro* formation of PGCLC. However, Zhu et al. found that the naive pluripotency gene *TFCP2L1* was not detectable in porcine PGC compared with human PGC [10], but was significantly expressed in the PGCLC differentiated from porcine SDSC. Consequently, PGCLC derived from porcine SDSC have germline characteristics consistent with human PGC [9, 10, 64], although the precise signaling mechanisms involved in their formation remain to be fully understood.

As reported in the introduction, the efficiency of inducing porcine SDSC to differentiate into PGCLC was found to be relatively low, at approximately 1.4% [25]. Considering that the quantity and quality of PGCLC are critical to the *in vitro* gametogenesis process, there is an urgent need to explore the key mechanisms that promote PGCLC production. Recent studies have demonstrated that endogenous metabolites possess the potential to control cellular fate [7, 26, 27]. Interestingly, by comparing the effects of various endogenous metabolites (LH, MLT and RA), we identified the MAPK signaling pathway may be the most central influencing factor in PGCLC proliferation (Figs. 8 and 9). Further evidence of DEGs at the differentiation stage (P2-4 to PGCLC) and the PGCLC highly expressed genes are significantly enriched in the MAPK cascaded-related biological functions (Fig. 5A). A whole-transcriptome analysis study showed that LH stimulates the proliferation of PGCLC through the hippo signaling pathway associated ceRNA network [26], indicating that the influence on PGCLC proliferation is not singular in nature. Nevertheless, how to ensure the quantity and quality of PGCLC required during *in vitro* gametogenesis remains a critical area for future research.

In conclusion, our results suggest for the first time that porcine SDSC with the multipotent differentiation potential and germline potential to induce PGCLC *in vitro* are derived from MDFP in the skin (Fig. 9). Moreover, the study highlights the transcriptional dynamics of porcine skin from *in vitro* culture to PGCLC and the role of the MAPK signaling pathway as a core inducer of PGCLC proliferation (Fig. 9). Importantly, porcine SDSC-induced PGCLC specification exhibits conservation with the core gene expression of the human PGC lineage. This work provides a reference for researchers engaged in the multipotent differentiation potential of SDSC and addresses several gaps in the study of the germline differentiation potential of porcine SDSC. Given that SDSC-derived PGCLC is expected to treat individuals with azoospermia or oocyte abnormalities, future research will focus on reconstituting the entire process of *in vitro* gametogenesis in order to further evaluate their potential as a therapeutic option for specific causes of infertility.

Declarations

Acknowledgments

This work was supported by National Natural Science Foundation of China (32072734 and 32100683), Natural Science Foundation (ZR2021QC003 and ZR2021QC041) and Taishan Scholar Construction Foundation (ts20190946 to Shen W., tsqn202211194 to Ge W.) of Shandong Province, China.

Author Contributions

Wen-Xiang Liu, Chun-Xiao Li, Xin-Xiang Xie, and Xiao-Feng Sun conducted the animal experiments; Wen-Xiang Liu, Wei Ge, and Tian Qiao analyzed the single-cell data; Wen-Xiang Liu and Chun-Xiao Li wrote the manuscript; Wei Shen and Shun-Feng Cheng designed the experiments. All authors read and approved the final manuscript.

Data availability

In this study, scRNA-seq data of porcine skin and skin-derived stem cells (SDSC) has been placed in the Genome Sequence Archive (GSA) of National Genomics Data Center (https://bigd.big.ac.cn) under the accession number CRA009222. Moreover, the accession number of transcriptome landscape of PGCLC derived from porcine SDSC is CRA009205. The RNA-seq data reported for PGCLC following LH or MLT exposure have been deposited in GSA with the accession number CRA009213.

Competing Interests

The authors have declared that no competing interest exists.

Ethics approval

The fetal pigs, CD-1 mice and CAG/eGFP transgenic mice used in this experiment are detailedly described in the materials and methods. Human fetal genital ridge tissue samples were from Anqiu Women and Children's Hospital, Shandong Province. According to national guidelines, all study participants obtained written informed consent. This study was conducted by the Ethics Committee of Anqiu Women's and Children's Hospital and the Ethics Committee of Qingdao Agricultural University (QAU; Agreement No. 2020-018).

References

1. Agarwal A, Mulgund A, Hamada A, Chyatte MR (2015) A unique view on male infertility around the globe. Reprod Biol Endocrinol 13:37 Epub 2015/05/01. 10.1186/s12958-015-0032-1
2. Qiao J, Wang ZB, Feng HL, Miao YL, Wang Q, Yu Y et al (2014) The root of reduced fertility in aged women and possible therapentic options: current status and future perspects. Mol Aspects Med 38:54–85 Epub 2013/06/26. 10.1016/j.mam.2013.06.001

3. Mouka A, Tachdjian G, Dupont J, Drevillon L, Tosca L (2016) In Vitro Gamete Differentiation from Pluripotent Stem Cells as a Promising Therapy for Infertility. Stem Cells Dev 25(7):509–521 Epub 2016/02/14. 10.1089/scd.2015.0230
4. Ge W, Chen C, De Felici M, Shen W (2015) In vitro differentiation of germ cells from stem cells: a comparison between primordial germ cells and in vitro derived primordial germ cell-like cells. Cell Death Dis 6(10) Epub 2015/10/16. 10.1038/cddis.2015.265. e1906
5. Hayashi K, Ohta H, Kurimoto K, Aramaki S, Saitou M (2011) Reconstitution of the mouse germ cell specification pathway in culture by pluripotent stem cells. Cell 146(4):519–532 Epub 2011/08/09. 10.1016/j.cell.2011.06.052
6. Zhou Q, Wang M, Yuan Y, Wang X, Fu R, Wan H et al (2016) Complete Meiosis from Embryonic Stem Cell-Derived Germ Cells In Vitro. Cell Stem Cell 18(3):330–340 Epub 2016/03/01. 10.1016/j.stem.2016.01.017
7. Liu WX, Tan SJ, Wang YF, Zhang FL, Feng YQ, Ge W et al (2022) Melatonin promotes the proliferation of primordial germ cell-like cells derived from porcine skin-derived stem cells: A mechanistic analysis. J Pineal Res 73(4):e12833 Epub 2022/09/16. 10.1111/jpi.12833
8. Zhao XY, Li W, Lv Z, Liu L, Tong M, Hai T et al (2009) iPS cells produce viable mice through tetraploid complementation. Nature 461(7260):86–90 Epub 2009/08/13. 10.1038/nature08267
9. Irie N, Weinberger L, Tang WW, Kobayashi T, Viukov S, Manor YS et al (2015) SOX17 is a critical specifier of human primordial germ cell fate. Cell 160(1–2):253–268 Epub 2014/12/30. 10.1016/j.cell.2014.12.013
10. Zhu Q, Sang F, Withey S, Tang W, Dietmann S, Klisch D et al (2021) Specification and epigenomic resetting of the pig germline exhibit conservation with the human lineage. Cell Rep 34(6):108735 Epub 2021/02/11. 10.1016/j.celrep.2021.108735
11. Grabole N, Tischler J, Hackett JA, Kim S, Tang F, Leitch HG et al (2013) Prdm14 promotes germline fate and naive pluripotency by repressing FGF signalling and DNA methylation. EMBO Rep 14(7):629–637 Epub 2013/05/15. 10.1038/embor.2013.67
12. Gutierrez K, Dicks N, Glanzner WG, Agellon LB, Bordignon V (2015) Efficacy of the porcine species in biomedical research. Front Genet 6:293 Epub 2015/10/07. 10.3389/fgene.2015.00293
13. Walters EM, Wells KD, Bryda EC, Schommer S, Prather RS (2017) Swine models, genomic tools and services to enhance our understanding of human health and diseases. Lab Anim (NY) 46(4):167–172 Epub 2017/03/23. 10.1038/laban.1215
14. Kobayashi T, Zhang H, Tang WWC, Irie N, Withey S, Klisch D et al (2017) Nature 546(7658):416–420 Epub 2017/06/14. 10.1038/nature22812. Principles of early human development and germ cell program from conserved model systems
15. Kanemura H, Go MJ, Shikamura M, Nishishita N, Sakai N, Kamao H et al (2014) Tumorigenicity studies of induced pluripotent stem cell (iPSC)-derived retinal pigment epithelium (RPE) for the treatment of age-related macular degeneration. PLoS ONE 9(1):e85336 Epub 2014/01/24. 10.1371/journal.pone.0085336

16. Golchin A, Chatziparasidou A, Ranjbarvan P, Niknam Z, Ardeshirylajimi A (2021) Embryonic Stem Cells in Clinical Trials: Current Overview of Developments and Challenges. Adv Exp Med Biol 1312:19–37 Epub 2020/11/08. doi: 10.1007/5584_2020_592. PubMed PMID: 33159303
17. Sun R, Sun YC, Ge W, Tan H, Cheng SF, Yin S et al (2015) The crucial role of Activin A on the formation of primordial germ cell-like cells from skin-derived stem cells in vitro. Cell Cycle 14(19):3016–3029 PubMed PMID: 26406115; PubMed Central PMCID: PMCPMC4825550
18. Ge W, Ma HG, Cheng SF, Sun YC, Sun LL, Sun XF et al (2015) Differentiation of early germ cells from human skin-derived stem cells without exogenous gene integration. Sci Rep 5:13822 Epub 2015/09/09. 10.1038/srep13822
19. Ge W, Cheng SF, Dyce PW, De Felici M, Shen W (2016) Skin-derived stem cells as a source of primordial germ cell- and oocyte-like cells. Cell Death Dis 7(11):e2471 Epub 2016/11/11. 10.1038/cddis.2016.366
20. Zheng Y, Du X, Wang W, Boucher M, Parimoo S, Stenn K (2005) Organogenesis from dissociated cells: generation of mature cycling hair follicles from skin-derived cells. J Invest Dermatol. ;124(5):867 – 76. Epub 2005/04/28. doi: 10.1111/j.0022-202X.2005.23716.x. PubMed PMID: 15854024
21. Sriram G, Bigliardi PL, Bigliardi-Qi M (2015) Fibroblast heterogeneity and its implications for engineering organotypic skin models in vitro. Eur J Cell Biol 94(11):483–512 .001. PubMed PMID: 26344860
22. Driskell RR, Lichtenberger BM, Hoste E, Kretzschmar K, Simons BD, Charalambous M et al (2013) Distinct fibroblast lineages determine dermal architecture in skin development and repair. Nature 504(7479):277–281 Epub 2013/12/18. 10.1038/nature12783
23. Ge W, Tan SJ, Wang SH, Li L, Sun XF, Shen W et al (2020) Single-cell Transcriptome Profiling reveals Dermal and Epithelial cell fate decisions during Embryonic Hair Follicle Development. Theranostics 10(17):7581–7598 Epub 2020/07/21. 10.7150/thno.44306
24. Ge W, Zhang W, Zhang Y, Zheng Y, Li F, Wang S et al (2021) A Single-cell Transcriptome Atlas of Cashmere Goat Hair Follicle Morphogenesis. Genomics Proteom Bioinf. Epub 2021/09/18 10.1016/j.gpb.2021.07.003
25. Linher K, Dyce P, Li J (2009) Primordial germ cell-like cells differentiated in vitro from skin-derived stem cells. PLoS ONE 4(12):e8263 Epub 2009/12/17. 10.1371/journal.pone.0008263
26. Zhang MY, Tian Y, Zhang SE, Yan HC, Ge W, Han BQ et al (2021) The proliferation role of LH on porcine primordial germ cell-like cells (pPGCLCs) through ceRNA network construction. Clin Transl Med 11(10):e560 PubMed PMID: 34709759; PubMed Central PMCID: PMCPMC8516341
27. Yan HC, Li L, Liu JC, Wang YF, Liu XL, Ge W et al (2019) RA promotes proliferation of primordial germ cell-like cells differentiated from porcine skin-derived stem cells. J Cell Physiol 234(10):18214–18229 Epub 2019/03/13. 10.1002/jcp.28454
28. A EM. Isolation and propagation of mouse embryonic fibroblasts and preparation of mouse embryonic feeder layer cells. Curr Protoc Stem Cell Biol. ;Chap. 1:Unit1C 3. Epub 2008/09/12. doi:

10.1002/9780470151808.sc01c03s3. PubMed PMID: 18785164

29. Stuart T, Butler A, Hoffman P, Hafemeister C, Papalexi E, Mauck WM 3 et al (2019) Cell 177(7):1888–1902 .e21. Epub 2019/06/11. 10.1016/j.cell.2019.05.031. Comprehensive Integration of Single-Cell Data
30. Street K, Risso D, Fletcher RB, Das D, Ngai J, Yosef N et al (2018) Slingshot: cell lineage and pseudotime inference for single-cell transcriptomics. BMC Genomics 19(1):477 Epub 20180619. 10.1186/s12864-018-4772-0
31. Liu WX, Donatella F, Tan SJ, Ge W, Wang JJ, Sun XF et al (2021) Detrimental effect of Bisphenol S in mouse germ cell cyst breakdown and primordial follicle assembly. Chemosphere 264(Pt 1):128445 Epub 2020/10/06. 10.1016/j.chemosphere.2020.128445
32. Liu WX, Tan SJ, Wang YF, Li L, Sun XF, Liu J et al (2020) Melatonin ameliorates murine fetal oocyte meiotic dysfunction in F1 and F2 offspring caused by nicotine exposure during pregnancy. Environ Pollut. ;263(Pt A):114519. Epub 2020/04/24. doi: 10.1016/j.envpol.2020.114519. PubMed PMID: 32325354
33. Livak KJ, Schmittgen TD (2001) Analysis of relative gene expression data using real-time quantitative PCR and the 2(-Delta Delta C(T)) Method. Methods 25(4):402–408 Epub 2002/02/16. 10.1006/meth.2001.1262
34. Yu G, Wang LG, Han Y, He QY (2012) clusterProfiler: an R package for comparing biological themes among gene clusters. Omics 16(5):284–287 Epub 20120328. doi: 10.1089/omi.2011.0118. PubMed PMID: 22455463; PubMed Central PMCID: PMCPMC3339379
35. Gupta K, Levinsohn J, Linderman G, Chen D, Sun TY, Dong D et al (2019) Dev Cell 48(1):17–31 PubMed PMID: 30595533; PubMed Central PMCID: PMCPMC6361530. Single-Cell Analysis Reveals a Hair Follicle Dermal Niche Molecular Differentiation Trajectory that Begins Prior to Morphogenesis
36. Deng CC, Hu YF, Zhu DH, Cheng Q, Gu JJ, Feng QL et al (2021) Single-cell RNA-seq reveals fibroblast heterogeneity and increased mesenchymal fibroblasts in human fibrotic skin diseases. Nat Commun 12(1):3709 Epub 2021/06/19. 10.1038/s41467-021-24110-y
37. Ascension AM, Fuertes-Alvarez S, Ibanez-Sole O, Izeta A, Arauzo-Bravo MJ (2021) Human Dermal Fibroblast Subpopulations Are Conserved across Single-Cell RNA Sequencing Studies. J Invest Dermatol 141(7):1735–1744 PubMed PMID: 33385399
38. Detmar M, Brown LF, Schon MP, Elicker BM, Velasco P, Richard L et al (1998) Increased microvascular density and enhanced leukocyte rolling and adhesion in the skin of VEGF transgenic mice. J Invest Dermatol. ;111(1):1–6. Epub 1998/07/17. doi: 10.1046/j.1523-1747.1998.00262.x. PubMed PMID: 9665379
39. Kaucka M, Szarowska B, Kavkova M, Kastriti ME, Kameneva P, Schmidt I et al (2021) Nerve-associated Schwann cell precursors contribute extracutaneous melanocytes to the heart, inner ear, supraorbital locations and brain meninges. Cell Mol Life Sci 78(16):6033–6049 Epub 2021/07/19. 10.1007/s00018-021-03885-9

40. Fung CW, Zhou S, Zhu H, Wei X, Wu Z, Wu AR (2022) Cell fate determining molecular switches and signaling pathways in Pax7-expressing somitic mesoderm. Cell Discov 8(1):61 Epub 2022/06/29. 10.1038/s41421-022-00407-0
41. Bondjers C, He L, Takemoto M, Norlin J, Asker N, Hellstrom M et al (2006) Microarray analysis of blood microvessels from PDGF-B and PDGF-Rbeta mutant mice identifies novel markers for brain pericytes. FASEB J. ;20(10):1703-5. Epub 2006/06/30. doi: 10.1096/fj.05-4944fje. PubMed PMID: 16807374
42. Garcia FJ, Sun N, Lee H, Godlewski B, Mathys H, Galani K et al (2022) Single-cell dissection of the human brain vasculature. Nature 603(7903):893–899 Epub 2022/02/15. 10.1038/s41586-022-04521-7
43. Pelekanou V, Villarroel-Espindola F, Schalper KA, Pusztai L, Rimm DL (2018) CD68, CD163, and matrix metalloproteinase 9 (MMP-9) co-localization in breast tumor microenvironment predicts survival differently in ER-positive and -negative cancers. Breast Cancer Res 20(1):154 Epub 2018/12/19. 10.1186/s13058-018-1076-x
44. Zhang Q, He Y, Luo N, Patel SJ, Han Y, Gao R et al (2019) Landscape and Dynamics of Single Immune Cells in Hepatocellular Carcinoma. Cell 179(4):829–845 e20. Epub 2019/11/02. 10.1016/j.cell.2019.10.003
45. Saxena N, Mok KW, Rendl M (2019) An updated classification of hair follicle morphogenesis. Exp Dermatol 28(4):332–344 Epub 2019/03/20. 10.1111/exd.13913
46. Fan A, Ma K, An X, Ding Y, An P, Song G et al (2013) Effects of TET1 knockdown on gene expression and DNA methylation in porcine induced pluripotent stem cells. Reproduction 146(6):569–579 Epub 2013/09/21. 10.1530/REP-13-0212
47. Pan Y, Liu Z, Shen J, Kopan R (2005) Notch1 and 2 cooperate in limb ectoderm to receive an early Jagged2 signal regulating interdigital apoptosis. Dev Biol 286(2):472–482 Epub 2005/09/20. 10.1016/j.ydbio.2005.08.037
48. Cortes F, Debacker C, Peault B, Labastie MC (1999) Differential expression of KDR/VEGFR-2 and CD34 during mesoderm development of the early human embryo. Mech Dev 83(1–2):161–164 Epub 1999/06/25. 10.1016/s0925-4773(99)00030-1
49. Barnes RM, Firulli BA, VanDusen NJ, Morikawa Y, Conway SJ, Cserjesi P et al (2011) Hand2 loss-of-function in Hand1-expressing cells reveals distinct roles in epicardial and coronary vessel development. Circ Res 108(8):940–949 Epub 2011/02/26. 10.1161/CIRCRESAHA.110.233171
50. Burtscher I, Lickert H (2009) Foxa2 regulates polarity and epithelialization in the endoderm germ layer of the mouse embryo. Development 136(6):1029–1038 Epub 2009/02/24. 10.1242/dev.028415
51. Tang WW, Dietmann S, Irie N, Leitch HG, Floros VI, Bradshaw CR et al (2015) A Unique Gene Regulatory Network Resets the Human Germline Epigenome for Development. Cell 161(6):1453–1467 Epub 2015/06/06. 10.1016/j.cell.2015.04.053

52. Betto RM, Diamante L, Perrera V, Audano M, Rapelli S, Lauria A et al (2021) Metabolic control of DNA methylation in naive pluripotent cells. Nat Genet 53(2):215–229 Epub 2021/02/03. 10.1038/s41588-020-00770-2
53. Okita K, Ichisaka T, Yamanaka S (2007) Generation of germline-competent induced pluripotent stem cells. Nature. ;448(7151):313-7. Epub 2007/06/08. doi: 10.1038/nature05934. PubMed PMID: 17554338
54. Sierra RA, Hoverter NP, Ramirez RN, Vuong LM, Mortazavi A, Merrill BJ et al (2018) TCF7L1 suppresses primitive streak gene expression to support human embryonic stem cell pluripotency. Development 145(4). 10.1242/dev.161075PubMed PMID: 29361574; PubMed Central PMCID: PMCPMC5869011 Epub 2018/01/24
55. Rossant J (2015) Mouse and human blastocyst-derived stem cells: vive les differences. Development. ;142(1):9–12. Epub 2014/12/18. doi: 10.1242/dev.115451. PubMed PMID: 25516964
56. Davidson KC, Mason EA, Pera MF (2015) The pluripotent state in mouse and human. Development. ;142(18):3090-9. Epub 2015/09/24. doi: 10.1242/dev.116061. PubMed PMID: 26395138
57. Kurimoto K, Saitou M (2018) Epigenome regulation during germ cell specification and development from pluripotent stem cells. Curr Opin Genet Dev 52:57–64 Epub 2018/06/17. 10.1016/j.gde.2018.06.004
58. Wei W, Qing T, Ye X, Liu H, Zhang D, Yang W et al (2008) Primordial germ cell specification from embryonic stem cells. PLoS ONE 3(12):e4013 Epub 2008/12/25. 10.1371/journal.pone.0004013
59. Zhang W, Liu HT (2002) MAPK signal pathways in the regulation of cell proliferation in mammalian cells. Cell Res 12(1):9–18 Epub 2002/04/11. 10.1038/sj.cr.7290105
60. Toma JG, Akhavan M, Fernandes KJ, Barnabe-Heider F, Sadikot A, Kaplan DR et al (2001) Isolation of multipotent adult stem cells from the dermis of mammalian skin. Nat Cell Biol 3(9):778–784 Epub 2001/09/05. 10.1038/ncb0901-778
61. Dyce PW, Zhu H, Craig J, Li J (2004) Stem cells with multilineage potential derived from porcine skin. Biochem Biophys Res Commun 316(3):651–658 Epub 2004/03/23. 10.1016/j.bbrc.2004.02.093
62. Jiang Y, Zou Q, Liu B, Li S, Wang Y, Liu T et al (2021) Atlas of Prenatal Hair Follicle Morphogenesis Using the Pig as a Model System. Front Cell Dev Biol 9:721979 Epub 2021/10/26. 10.3389/fcell.2021.721979
63. Sun YC, Ge W, Lai FN, Zhang RQ, Wang JJ, Cheng SF et al (2017) Oocyte-like cells induced from CD34-positive mouse hair follicle stem cells in vitro. J Genet Genomics 44(8):405–407 PubMed PMID: 28844672
64. Gao X, Nowak-Imialek M, Chen X, Chen D, Herrmann D, Ruan D et al (2019) Establishment of porcine and human expanded potential stem cells. Nat Cell Biol 21(6):687–699 Epub 2019/06/05. 10.1038/s41556-019-0333-2

Figures

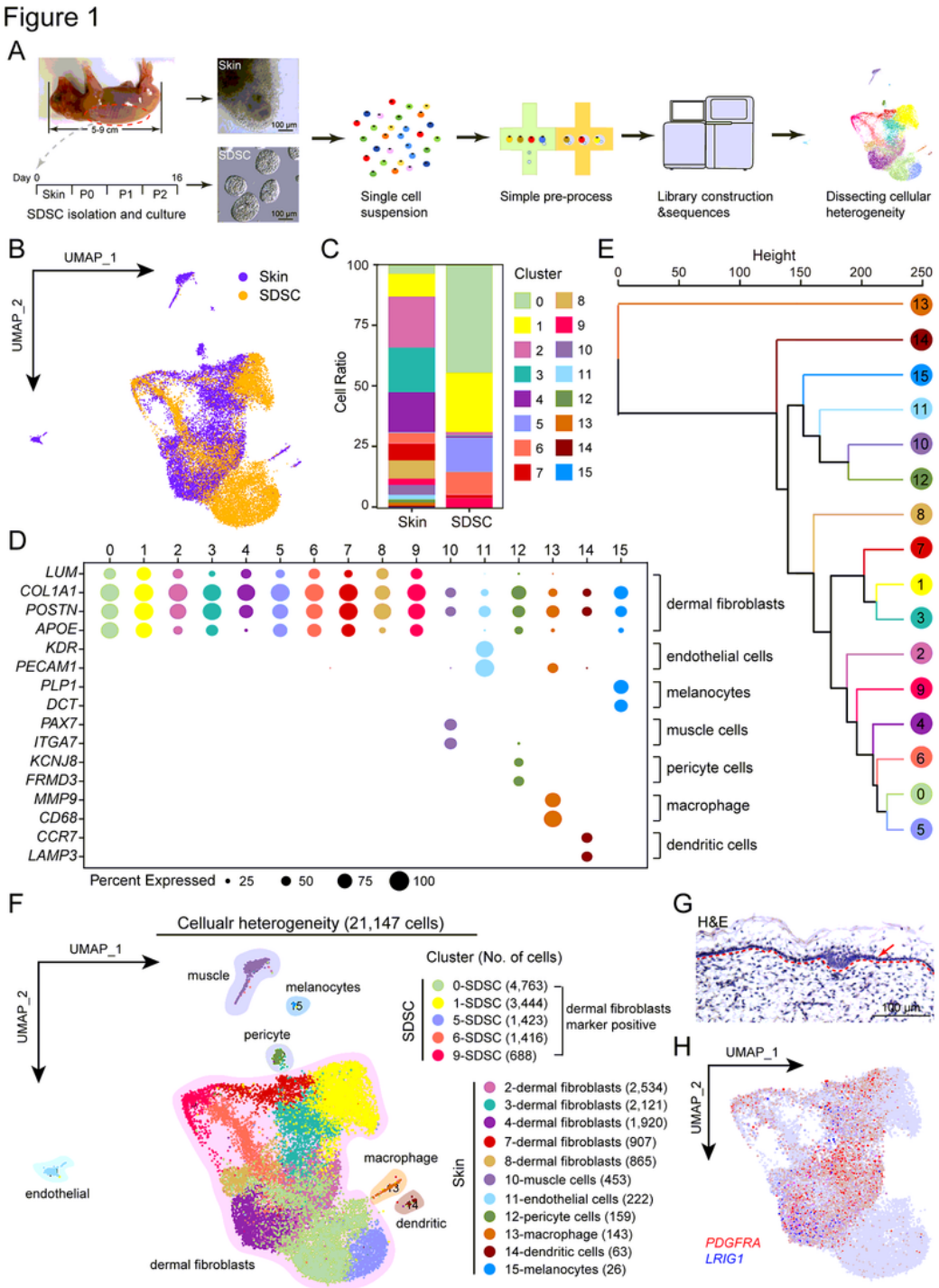

Figure 1

Analysis of single-cell transcriptome profiles of porcine dorsal skin and P2 skin-derived stem cells (SDSC)

(A) Diagram of sample preparation for single cell RNA sequencing (scRNA-seq). (B) uniform manifold approximation and projection (UMAP) plot color-coded by cell source. (C) Percentage of different cell clusters in porcine skin and SDSC. (D) Representative canonical cell type-specific marker expression

across all cell clusters. (E) Hierarchical clustering of different cell clusters identified by UMAP analysis. (F) UMAP projection of 21,147 single-cell profiles reveals 16 cell clusters in porcine skin and SDSC. (G) Representative image of H&E staining of porcine skin. Scale bar, 100 μm. (H) Feature plots of *PDGFRA*and *LRIG1* of dermal fibroblasts.

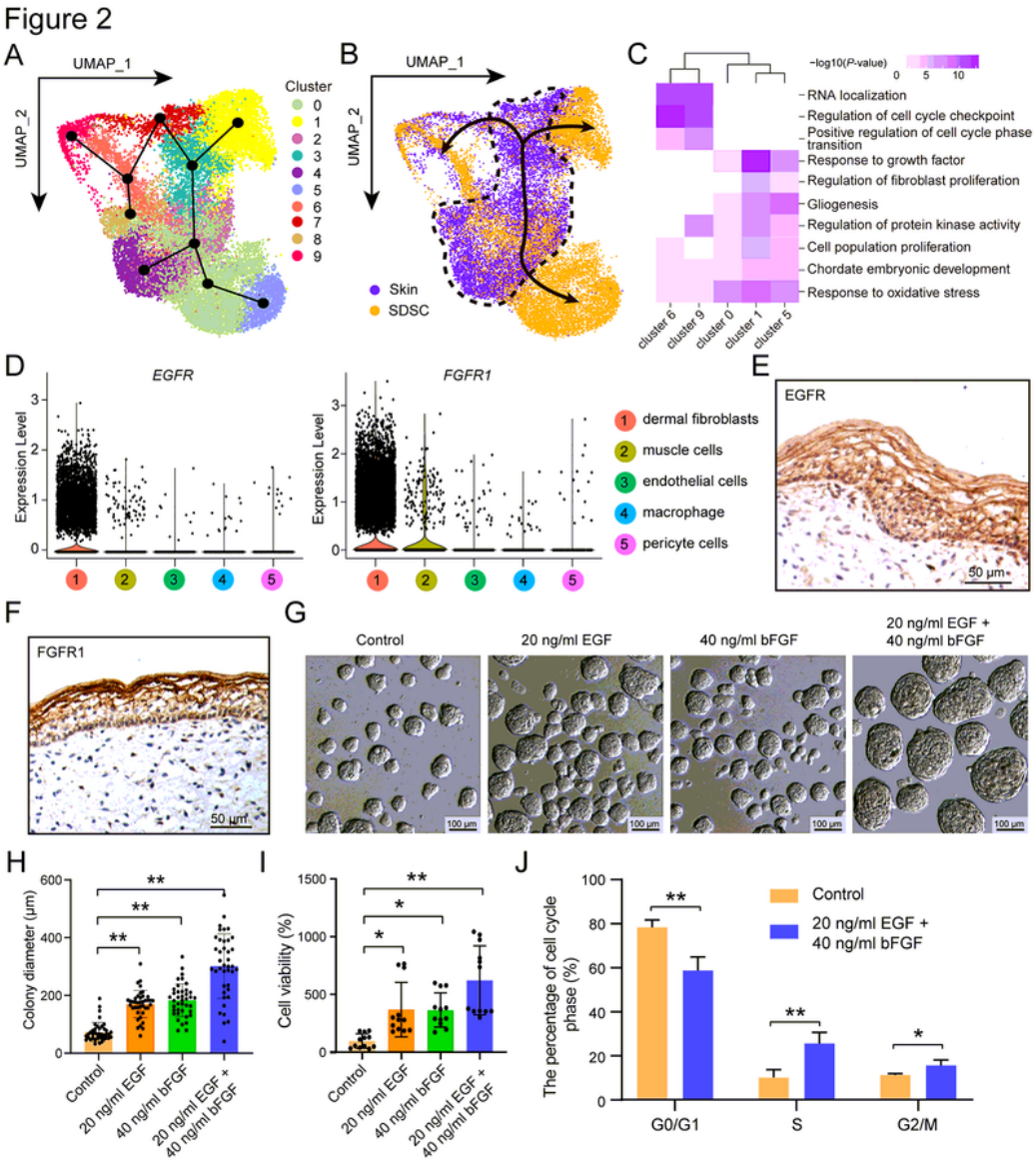

Figure 2

Growth factors (EGF/bFGF) are essential for the proliferation and formation of large SDSC colonies *in vitro*

(A) Slingshot analysis along the UMAP showed the root and terminal branches of the cell fates of dermal fibroblasts. (B) Slingshot infered the pseudotime trajectory in the P2 SDSC.(C) Heatmap demonstrating the gene ontology (GO) enrichment results of top 500 high expression genes in cell cluster 0, 1, 5, 6, 9 of SDSC. (D) Violin plots of the expression level of *EGFR* and *FGFR1* in porcine skin. (E) Immunohistochemical staining of EGFR in epidermal cells, hair follicles and dermal fibroblasts of the porcine skin. Scale bar, 50 μm.(F) Immunohistochemical staining of FGFR1 in epidermal cells, hair follicles and dermal fibroblasts of the porcine skin. Scale bar, 50 μm. (G) Morphology of SDSC colonies with or without EGF and/or bFGF. Scale bar, 100 μm. (H) Effects of EGF and bFGF on the diameter of P2 SDSC colonies. (I) Effects of EGF and bFGF on the cell viability of P2 SDSC colonies. (J) Effects of EGF and bFGF on the cell cycle of P2 SDSC colonies. The results are presented as mean ± SD. All the experiments were repeated at least three times. *: $0.01 < P < 0.05$; **: $P < 0.01$.

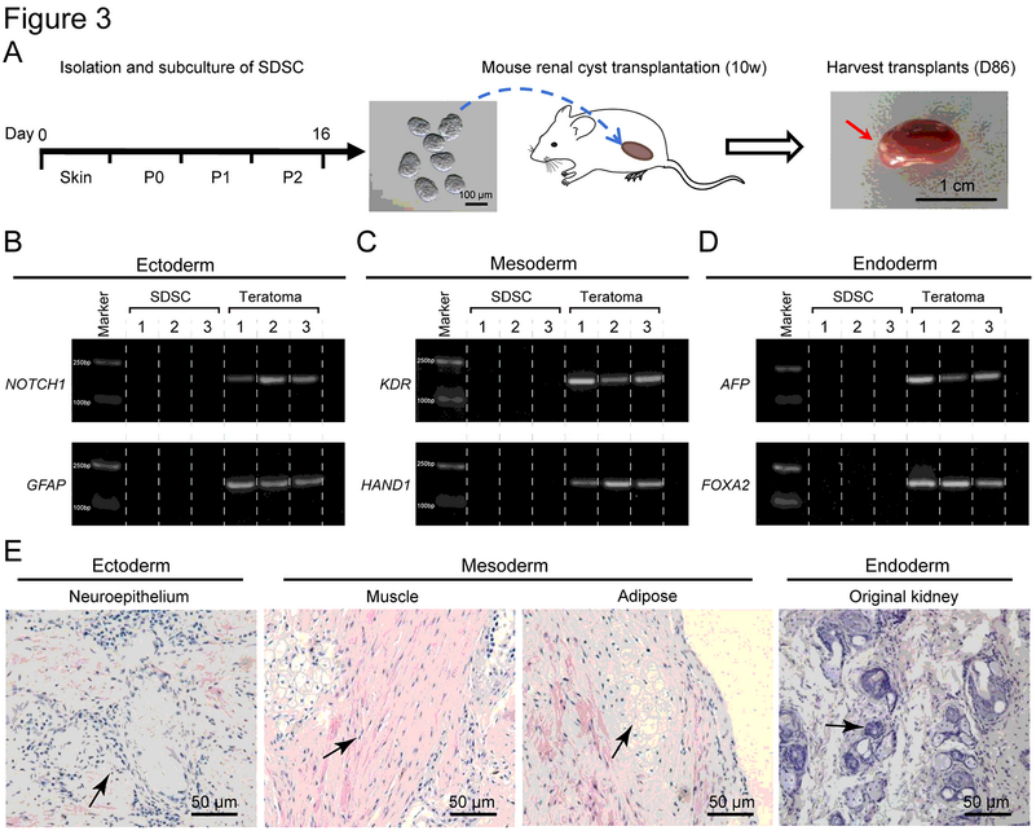

Figure 3

Teratoma experiment proved that SDSC was multipotent

(A) Schematic timelines and simplified protocols for the differentiation of the undifferentiated SDSC to the harvesting of the transplant under the kidney capsules of immune-deficient mice. (B) The expression of the ectodermal marker gene *NOTCH1* and *GFAP*in SDSC and teratoma was analyzed by PCR. (C) The

expression of the mesodermal marker gene *KDR* and *HAND1* in SDSC and teratoma was analyzed by PCR. (D) The expression of the endodermal marker gene *AFP* and *FOXA2* in SDSC and teratoma was analyzed by PCR. (E) Representative images of H&E staining of teratoma-like structures. Tumors contained tissues derived from three germ layers, including ectoderm-derived neuroepithelium, mesoderm-derived muscle and adipose, and endoderm-derived original kidney.

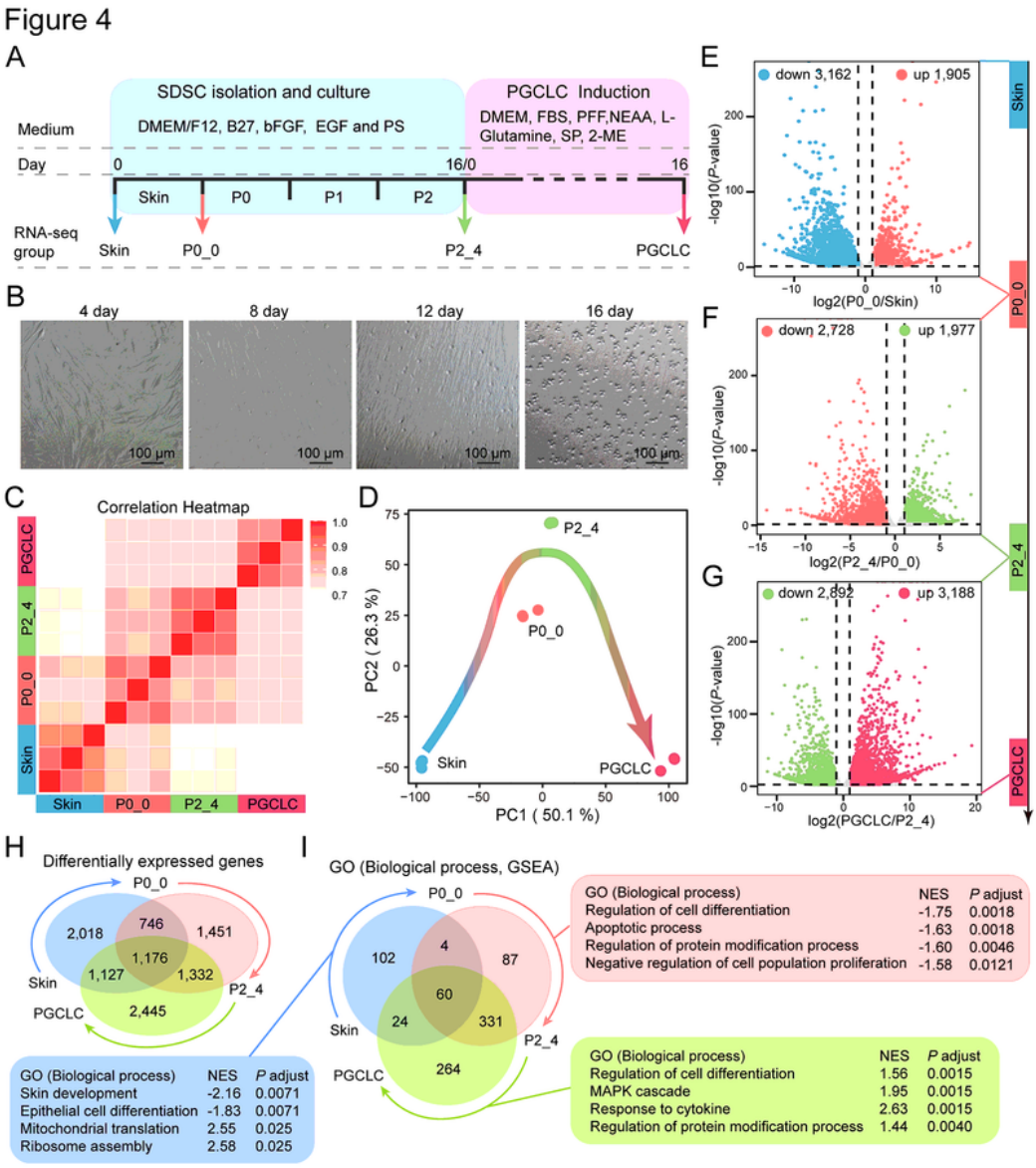

Figure 4

Transcriptional profiles with PGCLC induction from skin by RNA sequencing

(A) Scheme showing PGCLC induction from skin and scheme showing samples collection for transcriptional analysis. (B) Representative images of SDSC differentiation at 4 days, 8 days, 12 days, and 16 days. Scale bar, 100 μm. (C) Correlation matrix heatmap for skin group, P0_0 group, P2_4 group and PGCLC group. (D) Principal component analysis (PCA) for skin group, P0_0 group, P2_4 group and PGCLC group. (E) Volcano plots demonstrating the relationship between skin group and P0_0 group. (F) Volcano plots demonstrating the relationship between P0_0 group and P2_4 group. (G) Volcano plots demonstrating the relationship between P2_4 group and PGCLC group. (H) Venn diagram showed the number of DEGs for P0_0 *vs* skin, P2_4 *vs* P0_0 and PGCLC *vs* P2_4. (I) Representative GO biological processes obtained using GSEA analysis for P0_0 *vs* skin, P2_4 *vs* P0_0 and PGCLC *vs*P2_4. Venn diagram showed the number of GO biological processes items.

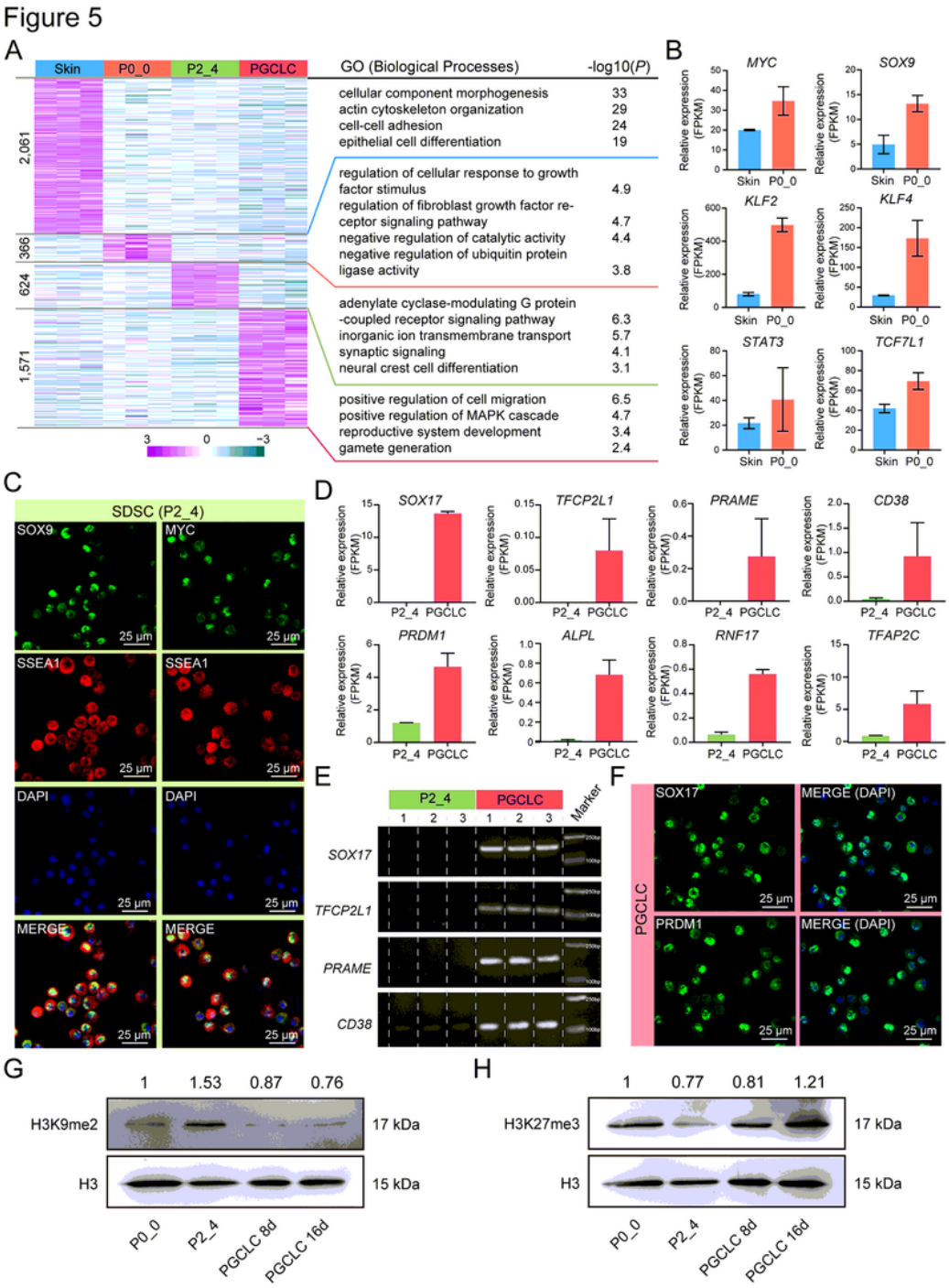

Figure 5

Transcriptional profiles and histone methylation modification during PGCLC induction indicates its PGC identity development

(A) Heatmap of gene expression of skin, P0_0, P2_4 and PGCLC showed different expression of genes in these four groups. Left, heatmap; right, GO biological processes items of 2,061, 366, 624 and 1,571 DEGs.

(B) Expression of pluripotent relative genes in skin group and P0_0 group. (C) Representative images of co-staining of P2_4 SDSC for SOX9/MYC (green) and SSEA1 (red). DAPI (blue) stained the nucleus. Scale bar, 25 μm. (D) Expression of PGC fate-related genes in P2_4 group and PGCLC group. (E) The expression of the PGC fate-related marker genes *SOX17*, *TFCP2L1*,*PRAME* and *CD38* in P2_4 groupand PGCLC groupwas analyzed by PCR. (F) Representative images of staining of PGCLC for SOX17 and PRDM1. DAPI (blue) stained the nucleus. Scale bar, 25 μm. (G) Western blotting analysis of H3K9me2 expression during PGCLC differentiation from multipotent dermal fibroblast progenitors (MDFP) derived SDSC. (H) Western blotting analysis of H3K27me3 expression during PGCLC differentiation from MDFP derived SDSC.

Figure 6

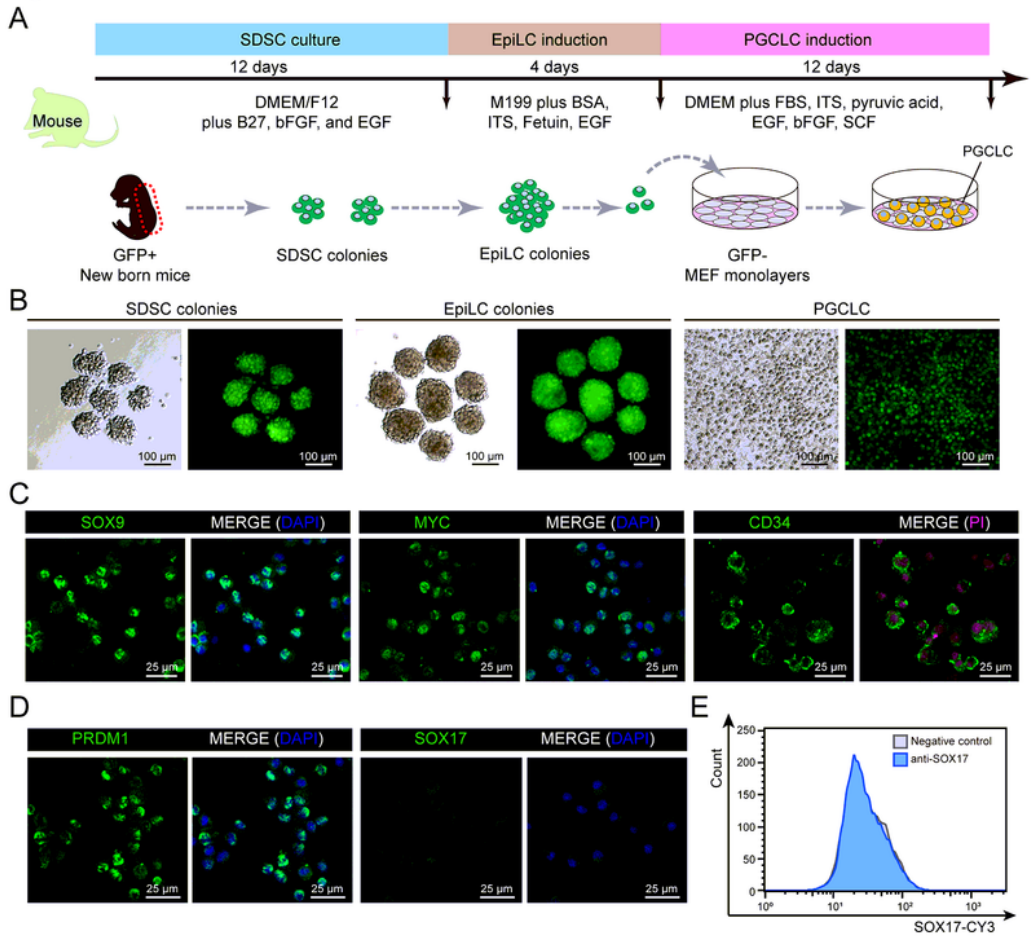

Figure 6

SOX17 was not detected in mouse SDSC-induced PGCLC

(A) A schematic diagram of the main steps to produce mouse PGCLC from mouse SDSC *in vitro*. (B) Representative images of mouse SDSC colonies, epiblast-like cells (EpiLCs) colonies and PGCLC. (C) Representative images of staining of mouse SDSC for SOX9, MYC and CD34 (green). DAPI (blue) or PI

(purple) stained the nucleus. (D) Representative images of staining of mouse PGCLC for PRDM1 and SOX17 (green). DAPI (blue) stained the nucleus. Scale bar, 25 μm. (E) Flow cytometry analysis of SOX17 on mouse PGCLC.

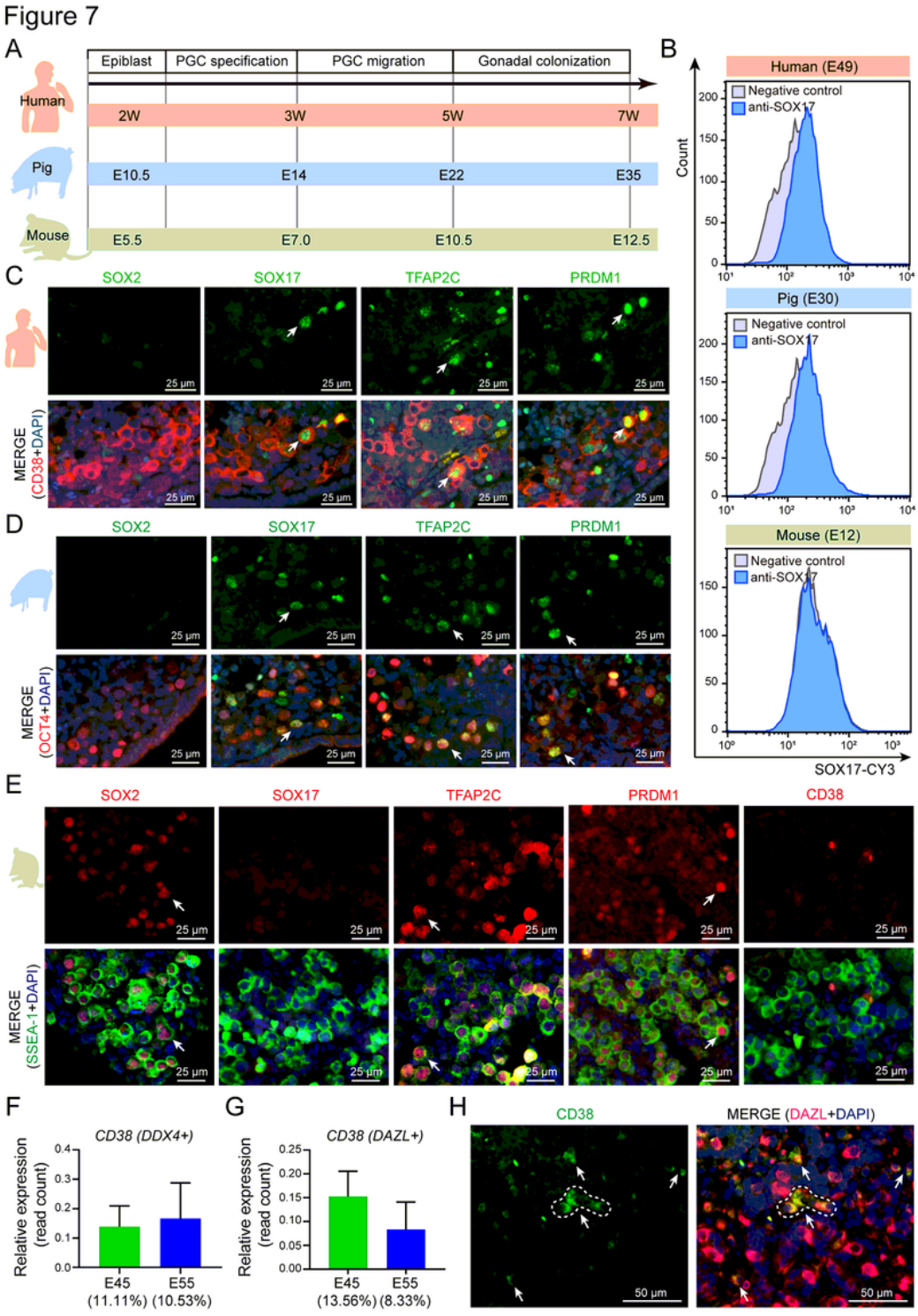

Figure 7

Porcine PGC share expression pattern with human PGC but different from mice

(A) Timeline of PGC origin and program in human, pig and mouse. (B) Flow cytometry analysis of SOX17 on genital ridges isolated from E49 human embryo, E30 pig embryo and E12 mouse embryo. (C) Representative images of co-staining for SOX2/SOX17/TFAP2C/PRDM1 (green) and CD38 (red) in E49 human gonadal PGC. DAPI (blue) stained the nucleus. Scale bar, 25 μm. (D) Representative images of co-staining for SOX2/SOX17/TFAP2C/PRDM1 (green) and OCT4 (red) in E30 porcine gonadal PGC. DAPI (blue) stained the nucleus. Scale bar, 25 μm. (E) Representative images of co-staining for SOX2/SOX17/TFAP2C/PRDM1/CD38 (red) and SSEA-1 (green) in E12 mouse gonadal PGC. DAPI (blue) stained the nucleus. Scale bar, 25 μm. (F) Single cell transcriptomic analysis showed double positive *CD38* and *DDX4*germ cells in E45 and E55 pig genital ridges. (G) Single cell transcriptomic analysis showed double positive *CD38* and *DAZL* germ cells in E45 and E55 pig genital ridges. (H) Representative images of co-staining of PGCLC for CD38 (green) and DAZL (red) in E45 porcine gonadal germ cell. DAPI (blue) stained the nucleus. Scale bar, 50 μm.

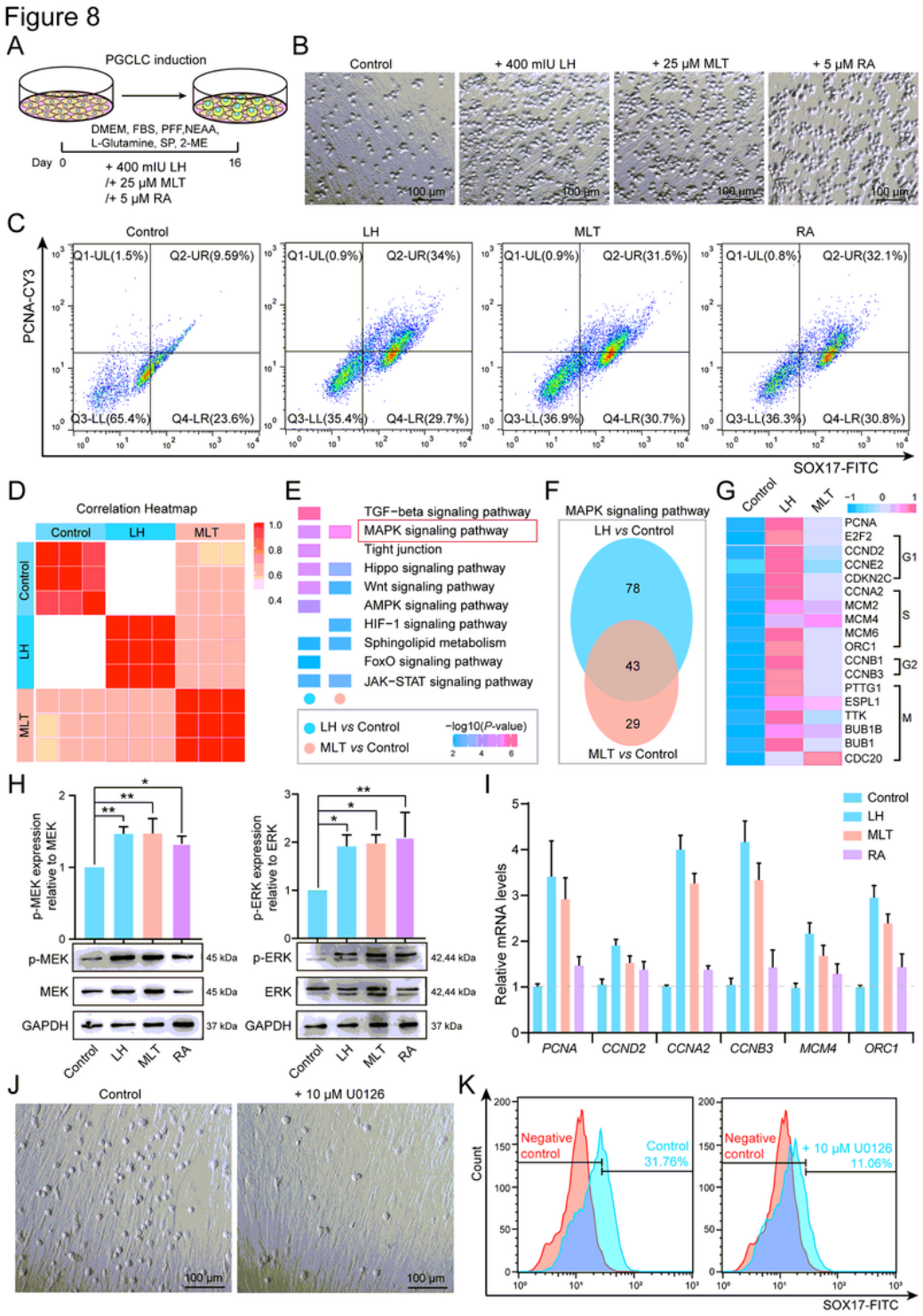

Figure 8

Activation of MAPK signaling pathway promoted the proliferation of PGCLC

(A) Schematic diagram of the research design. (B) Brightfield of cultures with 400 mIU LH, 25 μM MLT or 5 μM RA for 16 days. Scale bar, 100 μm. (C) Flow cytometry analysis of SOX17 (FITC) and PCNA (CY3) double staining with 400 mIU LH, 25 μM MLT or 5 μM RA. (D) Correlation matrix heatmap for control

group, LH group and MLT group. (E) The KEGG pathway enrichment of DEGs for LH *vs* control group and MLT *vs* control. (F) Venn diagram showed the number of enriched genes in MAPK signal pathway for LH *vs* control group and MLT *vs* control. (G) Heatmap analysis of DEGs associated with cell proliferation and cell cycle for LH *vs* control group and MLT *vs* control. (H) The protein levels of the p-MEK (MEK) and p-ERK (ERK) detected by WB in culturing with LH, MLT or RA groups for 16 days. (I) The expression levels of proliferation-related genes were detected by RT-qPCR in culturing with LH, MLT or RA groups for 16 days. (J) Brightfield of 10 μM U0126 culture for 16 days. Scale bar, 100 μm. (K) Flow cytometry analysis of SOX17 (FITC) staining with 10 μM U0126. The results are presented as mean ± SD. All the experiments were repeated at least three times. *: $0.01 < P < 0.05$; **: $P < 0.01$.

Figure 9

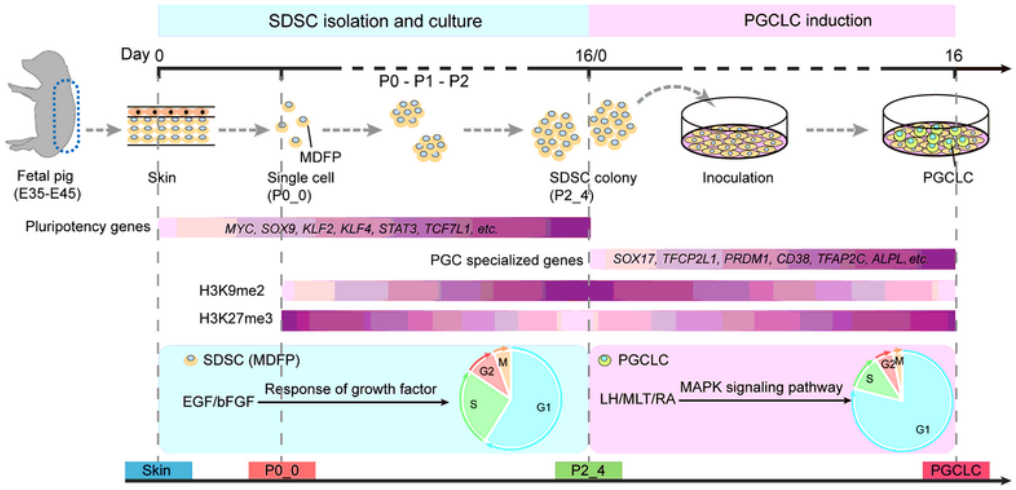

Figure 9

Schematic diagram of the germline potential of porcine skin-derived MDFP *in vitro*

In this study, single cell transcriptome analysis showed that porcine SDSC with germline potential to induce PGCLC *in vitro* are derived from MDFP in the skin. These cells are highly expressed pluripotent related genes (*MYC*, *SOX9*, *KLF2*, *KLF4*, *STAT3*, *TCF7L1*, *etc*), and actively responded to growth factors

(EGF/bFGF) stimulation to promote cell population proliferation. In the PGCLC induction program, PGC specialized related markers (*SOX17*, *TFCP2L1*, *PRDM1*, *CD38*, *TFAP2C*,*ALPL*, *etc*) begins to be expressed accompanied by epigenetic changes in histone methylation (H3K9me2, H3K27me3). Moreover, this study also highlights that MAPK signaling pathway is key to endogenous metabolites (LH/MLT/RA) promoting cell cycle related gene expression and proliferation in PGCLC.

Supplementary Files

This is a list of supplementary files associated with this preprint. Click to download.

- FigureS1.tif
- FigureS2.tif
- FigureS3.tif
- Supplementaryfigurelegends3.16.docx
- TableS1.xlsx
- TableS2.xlsx
- TableS3.xlsx
- TableS4.xlsx
- TableS5.xlsx
- TableS6.docx
- TableS7.docx